Research Report

Shell Mold Cracking and Its Prediction during the Casting of AC4C Aluminum Alloy

Shuxin Dong, Yasushi Iwata, Hiroshi Hohjo, Hiroaki Iwahori, Takashi Yamashita and Haruyoshi Hirano

Report received on Oct. 12, 2011

ABSTRACT The mechanism of shell mold cracking and its prediction during the casting of an aluminum alloy were elucidated. A cylindrical shell mold made of silica sand will fracture easily when filled with an aluminum alloy melt. The cracking mechanism is as follows. The inner surface of the shell mold undergoes a sudden temperature rise caused by contact with the melt, and attempts to expand. This thermal expansion is restrained by the rest of the mold, which is still at a lower temperature. Consequently, compressive stress develops near the inner surface, and tensile stress develops near the outer surface, causing the shell mold to fracture once the tensile stress exceeds the tensile strength of the shell mold. If a portion of a cylindrical shell mold is cut to reduce its thickness, a higher tensile stress act on the outer surface of this thinner region, and a crack will form more quickly after the mold is filled with an aluminum alloy melt. The relation of fracture stress and effective volume based on Weibull's statistical method, which is utilized for evaluating the strength of brittle materials, was obtained from the statistical properties of the tensile strength of the shell mold material. The criterion for shell mold cracking, enabling us to predict the shell mold cracking, can be described by the relation of fracture stress and effective volume.

KEYWORDS Shell Mold, Crack, Fracture Stress, Effective Volume, Prediction, Veining Defect, Casting, Aluminum, Alloy, Weibull's Statistical Method

1. Introduction

Components with intricate cavities, such as the cylinder heads of automobiles, can be cast as a single piece, without requiring assembly. In this casting, core molds made of shell molds or organic self-hardening sand are used in conjunction with a main mold to form complex cavities. However, if a crack occurs in the core mold during casting, the resulting cylinder head may be defective because of burrs or fins formed by the solidification of melt penetrating the crack. Such burrs or fins, commonly referred to as veining defects, are difficult to detect and remove. Therefore, it is important to choose an appropriate casting design and conditions that can avoid such defects in foundry production.

Generally encountered in sand mold castings along with metal penetration, pinholes, and blowholes, veining defects often occur in sand molds that contain organic binders. Campbell[1] proposed that veining defects originate from the thermal expansion of sand molds because of heating by the melt, but it remained unclear how much thermal expansion can occur before sand mold cracking occurs and when these cracks will appear during casting. Makiguchi[2] suggested that veining defects occur when the binder, grain size, filling state of the sand, or pouring temperature of melt are inappropriate, and that cracking is also influenced by the shape and dimension of the casting. Oda[3] argued that the thermal expansion coefficient of the sand has little to do with veining defects. Several methods of preventing veining defects have been reported. One of these is the addition of substances that react with the sand to form a glassy material.[4] Another is the mixing of boric acid or other substances with the sand to improve the deformability of the surface layer of the sand mold at elevated temperatures,[5] or adding Fe_2O_3 to the sand.[6,7] Coatings that can seal cracks on the surface of the sand mold by softening at elevated temperatures are commercially available. However, the above methods and products for the prevention of veining defects are mainly intended for cast iron or cast steel, and the complete prevention of veining defects remains a significant challenge.

In the past few decades, simulation technology for foundry engineering has made remarkable progress. The prediction of casting quality and die design are being conducted flourishingly based on numerical analysis of mold filling and solidification in various foundries.[8,9] Nevertheless, simulation techniques for

sand molds and cores, such as the prediction of veining defects, will remain under development until the mechanical models of sand molds and the cracking mechanism of the mold surface can be adequately understood.

In the present research, the thermo-mechanical behavior of shell molds heated by the melt during casting was investigated as it relates to mold surface cracking. A criterion for cracking is proposed, and predictions based on this criterion were investigated in the actual foundry production of cylinder head castings.

2. Experimental Method

2. 1 Casting Experiments

The cup-shaped experimental shell mold shown in **Fig. 1** was formed with an inside diameter of 60 mm, a height of 120 mm, and a thickness of 10 mm. The shell mold was formed in a steel mold using resin-coated sand (RCS) that was prepared by mixing JIS100 silica sand (99.8% SiO_2) with 1.5 mass% phenolic resin followed by curing at 300°C. The mold cracking was examined after pouring a JIS-AC4C aluminum alloy (hereafter called AC4C alloy) melt at 700°C into the cup-shaped experimental mold with a filling time of about 3 seconds. The effect of mold wall thickness on cracking was investigated by vertically grinding a part of the mold wall to various thicknesses. To investigate the effect of the pouring method on cracking, the following pouring experiments were also carried out.

1) Pouring to the inner or outer side of the mold only, so that only the inner or outer side contacted the melt.
2) Pouring to the inner and outer sides of the mold simultaneously, so that both sides contacted the melt at the same time.
3) Pouring to the inner and outer sides of the mold with a time lag, so that the inner side contacted the melt prior to the outer side, or vice versa.

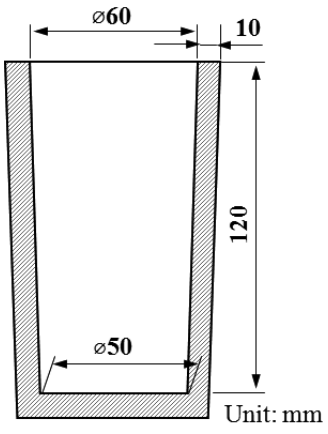

Fig. 1 Experimental cylindrical shell mold.

The mold used for these experiments was a 40-mm-high cylindrical mold cut from the upper part of the cup-shaped mold shown in Fig. 1. The filling time was 1 second for both the inner side and outer side of the mold.

The strain generated in the cup-shaped mold during pouring was measured by installing strain gauges around the circumference of the outer surface of the mold at a height of 60 mm above the bottom. To avoid the dissipation of the strain gauge adhesive into the grain interstitials of the mold, a high-viscosity adhesive was used. A high-temperature strain gauge, ZFLA-3 (Tokyo Sokki Kenkyujo Co., Ltd.) was used in the above measurements. The occurrence and propagation of the cracks were recorded by a high-speed camera with a recording speed of 1×10^5 fps.

2. 2 Thermal Stress Analysis of the Sand Mold

Coupled thermo-mechanical analysis of the mold was carried out with the commercial structural analysis code MSC MARC in two or three dimensions, depending on the purposes. To examine the relationship between stress and mold cracking during pouring, a two-dimensional thermo-mechanical analysis was conducted using a ring-shaped model to represent a horizontal cross section of the mold. It was necessary to calculate the temperature variation in the mold with a high accuracy in order to correctly determine the stress distribution. Besides measuring the thermal properties of the mold, the heat transfer coefficient at the interface between the melt and the mold surface was determined by the following method. A cup-shaped mold was made for temperature measurement. This mold had ⌀0.1 mm chromel-alumel thermocouples embedded at three positions along the thickness direction of the mold wall, with an interval of approximately 2.5 mm and at a height of 60 mm from the bottom of the mold. The correct positioning of the thermocouples was confirmed by X-ray transmission photography before pouring and the temperatures of the three points were measured during pouring. In the present study, the melt-mold interface heat transfer coefficient during the first 30 seconds was

considered significant because all of the observed mold cracks occurred within 30 seconds of melt pouring. The heat transfer coefficient was calculated to be 0.05 cal·cm^{-2}·°C^{-1}·s^{-1} by an inverse method, in which the heat transfer coefficient giving the nearest calculated temperatures to the measured results was chosen as the correct heat transfer coefficient. In the above thermal calculations of the heat transfer coefficient, a two-dimensional analysis was adopted. The time at which the melt surface within the mold arrived at the position of the embedded thermocouples during pouring was taken as the starting time of the analysis. The heat transfer coefficient of the mold-air interface was taken as 0.0008 cal·cm^{-2}·°C^{-1}·s^{-1}.

A three-dimensional analysis taking into account the filling process of the melt was also carried out to calculate the temperature and stress distributions in the cup-shaped mold. To describe the gradual heating process of the mold correctly during the 3 seconds of melt filling, the 120 mm height of the mold cavity was divided equally into 24 sections. Each ring-shaped section had a height of 5 mm and a heat transfer boundary condition with a heat transfer coefficient of 0.05 cal·cm^{-2}·°C^{-1}·s^{-1}. An environmental temperature of 700°C was applied section-by-section with a time lag of 0.125 seconds along the inner surface of the ring-shaped mold, starting from the bottom and arriving at the top 3 seconds later. The object of the above thermo-mechanical analysis was taken as the mold only and the radiation heat transfer of the melt surface in the mold was ignored.

Analysis of the 40-mm-high cylinder-shaped mold was performed using a two-dimensional model consisting of the mold and melt but ignoring the filling time of 1 second.

Table 1 Thermal and mechanical properties of the shell mold used for thermal and mechanical simulations.

Density (kg·m^{-3})	1.55×10^{3}
Thermal conductivity (W·m^{-1}·°C^{-1})	0.70
Specific heat (J·kg^{-1}·°C^{-1})	1.13×10^{3}
Linear thermal expansion coefficient (°C^{-1})	1.16×10^{-5}
Tensile strength, σ_t (MPa)	3.15
Compressive strength, σ_c (MPa)	10.44
Modulus of elasticity, E (GPa)	3.72
Poisson's ratio (-)	0.20

The thermal and mechanical properties of the mold are shown in **Table 1**. The mechanical properties were acquired by tensile and compressive tests using dumbbell-shaped planar specimens (5.5 mm in thickness, 25 mm in width, 75 mm in gauge length, and a transition radius of 30 mm) and columnar specimens (20 mm in diameter, 40 mm in length) respectively. The specimens were made from the same sand and cured under the same conditions as the molds.

The mechanical properties of the mold at elevated temperatures were estimated through extrapolating the room temperature properties according to the temperature dependence of the three-point bending strength, which was measured by a series of bending tests from room temperature to 400°C. The stress-strain curves at room temperature were measured using a video camera strain gauge. The thermal conductivity, specific heat, density, and thermal expansion coefficient of the mold were measured by box probe method, vacuum bottle method, bulk density method, and JACT M-2 test method (Japan Association of Casting Technology), respectively.

The stress-strain behavior of the mold was assumed to be as illustrated in **Fig. 2** for the thermo-mechanical analysis. The modulus and compressive yield stress of the mold were taken as the measured values given in Table 1. As was described in section 3.5, the tensile strength of the mold varied considerably with changes in effective volume, and so the stress-strain relationship under tension was assumed to be that of an ideal elastic material.

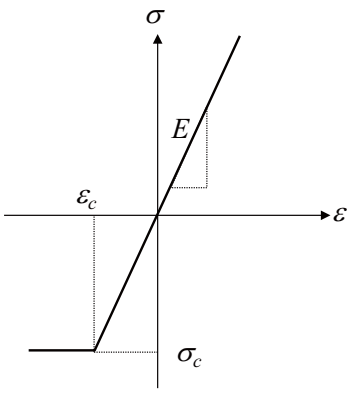

Fig. 2 Stress-strain model of the shell mold used for mechanical simulation.

3. Experimental Results and Discussion

3. 1 Cracking and Thermal Stress of the Experimental Mold

Figure 3 shows an example of cracking after pouring an AC4C alloy melt into the cup-shaped mold of Fig. 1. A crack began to propagate in the vertical direction of the mold wall accompanied by a sound, and the melt in the mold flowed out through the crack about 8 to 12 seconds after the start of pouring.

The calculated temperature and stress distributions in the mold wall along the thickness direction after contacting the melt are illustrated in **Fig. 4**. The inner surface of the mold underwent a rapid temperature rise upon contacting the melt, but the interior of the mold wall changed temperature much more slowly due to the low thermal conductivity of the sand. The outer surface of the mold, which was 10 mm away from the inner surface, showed almost no temperature change in the 10 seconds after pouring. The thermal stress distribution arising from the above temperature changes in the mold caused a tensile stress at the outer side and a compressive stress at the inner side of the mold wall in contact with the melt. The tensile stress at the outer side increased rapidly after pouring, because of thermal expansion of the silica sand of the mold, which had a linear thermal expansion coefficient of 1.16×10^{-5}°C^{-1}. The inner side of the mold wall expanded rapidly upon contact with the melt, while the outer side of the mold wall did not undergo thermal expansion because of the low thermal conductivity of the mold. Therefore, the thermal expansion of the heated inner area was constrained by the outer area, resulting in a compressive stress at the inner side and a tensile stress at the outer side of the mold wall. With time, the area of the heated inner side increased, and the area of the outer side decreased. The tensile stress at the outer side increased to match the compressive stress in the cross section. Cracking should occur when the tensile stress at the outer side exceeds the tensile strength of the mold. As shown in Fig. 4, the tensile stress reached the tensile strength (ranging from 2.16 to 3.87 MPa, averaging 3.15 MPa) 8 seconds after the start of pouring. In experiments, cracking occurred 8 to 12 seconds after the start of pouring. The cracking time calculations included some errors, because the above thermo-mechanical simulation was conducted using a two-dimensional model, and there were measurement errors in the determination of the mold properties, and the unevenness of the sand filling during preparing the mold. Nevertheless, the calculated cracking time agreed well with the measured value. A set of three representative strain curves measured using a cup-shaped mold with strain gauges installed at three circumferential positions around the outer surface is shown in **Fig. 5**. When the inner surface was heated by the melt, the tensile strains at the three positions around the outer surface of the mold began to increase. A crack occurred at a strain of about 500μ approximately 10 seconds after starting to pour. The strains at all three positions dropped simultaneously when the crack occurred. As shown in Fig. 5, the calculated and measured strains showed the same increasing tendency, although the measured values were lower than the calculated values. The fluctuation of approximately 100μ between the strains measured at the three positions may have resulted from unevenness

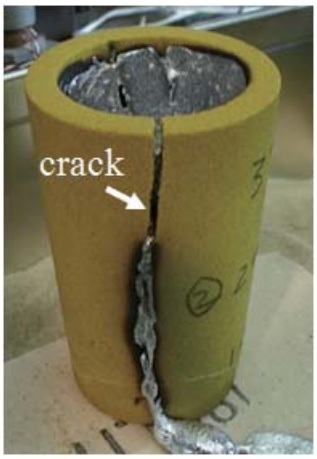

Fig. 3 A crack in the cylindrical shell mold.

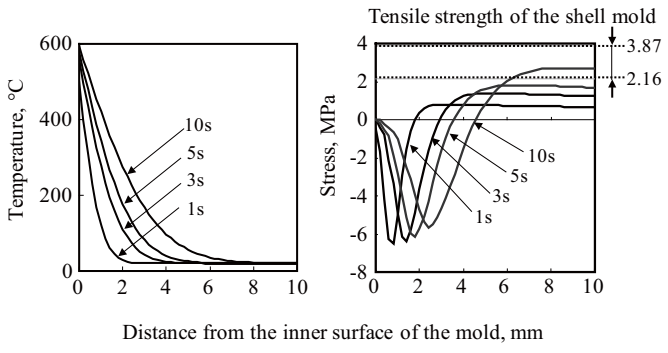

Fig. 4 Temperature and stress distributions along the thickness direction in the cross section of the cylindrical mold (two-dimensional analysis).

of the gauge adhesive, non-uniform filling of the sand, or other structural irregularities.

3. 2 The Effect of Pouring Method on Thermal Stress and Cracking

As discussed in the previous section, a crack appeared on the surface of the mold because the thermal stress exceeded the tensile strength of the mold. The relationship between thermal stress and cracking was further investigated by employing several different pouring methods. In the first method, an AC4C alloy melt was poured onto only the inner or outer surface of the ring-shaped mold described in section 2.1. In the second method, an AC4C alloy melt was poured onto both the inner and the outer surfaces simultaneously. In the third method, an AC4C alloy melt was first poured onto one surface, and then onto the other before any cracking, with a surface-to-surface time lag of 6 seconds. When using the first pouring method, a crack would occur at the side opposite from the pouring; that is, if the melt was poured onto the inner surface, the outer surface would crack, and vice versa. When using the second and the third methods, no cracks were observed. The temperature and stress distributions along the thickness direction of the mold wall, calculated using a two-dimensional model of the third filling method, are illustrated in **Fig. 6**. Although a tensile stress existed at the outer surface of the mold wall 5 seconds after melt filling of the inside of the mold, the stress changed to a compressive stress at 6.5 seconds once the melt had been poured onto the outside of the ring-shaped mold. The region under compressive stress continued to spread towards the center of the mold wall with time. The tensile stress of the central part in the thickness direction of the mold wall entered the tensile strength range at some time, but no crack was observed. Immediately upon pouring the melt by the second method, in which AC4C was poured onto the inner and outer surfaces of the mold at the same time, compressive stresses appeared at both the inner and outer surfaces, while tensile stress developed in the interior of the mold wall. The above experimental and simulation results suggest that cracks will occur if the tensile stress at mold surface exceeds the tensile strength, and that no crack will appear if the stresses at the surfaces are compressive, even if the tensile stresses within the mold wall exceed the tensile strength of the mold.

3. 3 Crack Origins

Stress distributions in a cup-shaped mold with a part of the wall vertically ground to a thickness of 5 mm are shown in **Fig. 7**. The mold shown in Fig. 7(a) was fully filled, while the mold shown in (b) was partly filled to a position 20 mm from the top edge of the mold. In Fig. 7(a), the highest stress acted on the lower area of the outer surface of the mold 2.8 seconds after the beginning of filling, but the point of the highest stress then migrated to the upper edge of the mold over the next few seconds as the filling continued. A crack appeared in the mold 5 to 6 seconds after the beginning

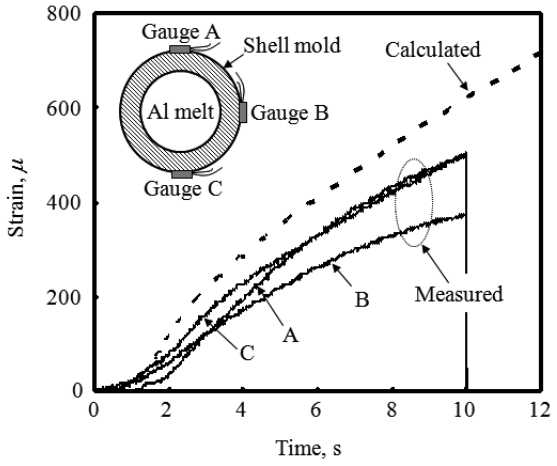

Fig. 5 Comparison of measured and calculated strains in the outer surface 60 mm above the bottom of the cylindrical shell mold from the start of pouring (three-dimensional analysis).

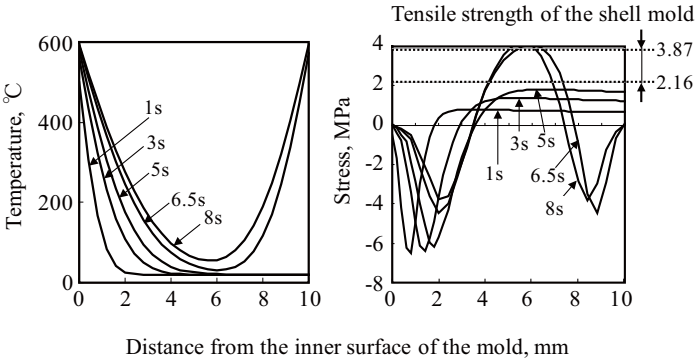

Fig. 6 Temperature and stress distributions along the thickness direction in the cross section of the ring-shaped shell mold contacting the melt at both surfaces, but with a time lag of 6 seconds (two-dimensional analysis).

of filling. The cracking time differed from that shown in Fig. 4, for reasons that will be discussed in the following section (3.4). Using a high-speed camera, the crack was observed to initiate at the upper edge and then propagate toward the bottom of the mold. In Fig. 7(b), the highest stress acted on the lower area of the mold, and the position of highest stress moved very little during the filling process. Under these filling conditions, the initial crack occurred approximately 15 seconds after the beginning of filling, and the crack was clearly observed to propagate toward the upper part of the mold. That is to say, for condition (a), the upper and lower parts of the mold developed comparatively high stresses, and the stress at the upper part exceeded the tensile strength of the mold at the time the crack occurred. For condition (b), the peak stress occurred only in the lower part of the mold throughout the filling process, and the stress in this area greatly exceeded the tensile strength of the mold when the crack initiated.

3. 4 The Effect of Mold Shape on Cracking Stress

In a mold with a thinly ground region 5 mm thick, as shown in Fig. 7(a), a crack occurred 5 to 6 seconds after the beginning of melt filling. To investigate the effect of the thinly ground region on cracking, regions on several different molds were ground to thicknesses varying from 10 mm (not ground) to 3 mm, and pouring experiments were carried out. In all cases, cracks occurred in the thinly ground region. These cracks appeared approximately 7 seconds, 5.5 seconds, and 4 seconds after the beginning of melt filling for ground thicknesses of 8 mm, 5 mm, and 3 mm, respectively. The cracks appeared sooner in more thinly ground parts.

The strains generated in the surfaces of molds before cracking were measured, as shown in **Fig. 8** for thinly ground parts of different thickness. For the unground mold, the strain was about 500μ at all the three measured points when the crack occurred. However, with decreasing thickness of the thinly ground parts, the strain in the thinly ground region became higher and the strain in the other regions became lower when the crack occurred. When the ground region was thinner than 5 mm, the strain in the ground region rose rapidly with decreasing thickness, and the strain for a thickness of 3 mm reached 3000μ. The mean tensile strength of the mold was determined to be 3.15 MPa by N = 10 tensile tests, as shown in Table 1. The tensile strength ranged from 2.16 MPa to 3.87 MPa, and the corresponding facture strain ranged from 580μ to 1040μ. That is to say, the strain of 3000μ measured in a mold with a thickness of 3 mm in the thinly ground region reached three times the fracture strain of the mold. In the above experiments, it was observed that in the unground mold with an even wall thickness of 10 mm, the strain was distributed evenly around the

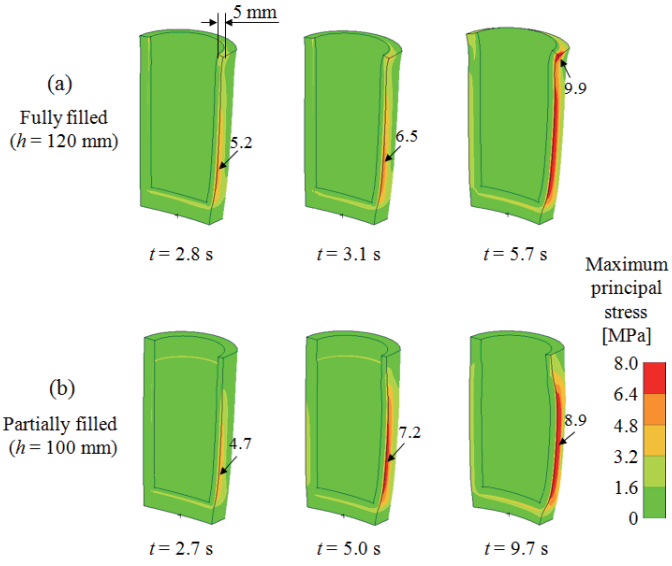

Fig. 7 Stress distributions within cylindrical shell molds (a) fully filled with the melt, and (b) only partially filled with the melt (100-fold amplified deformation, three-dimensional analysis).

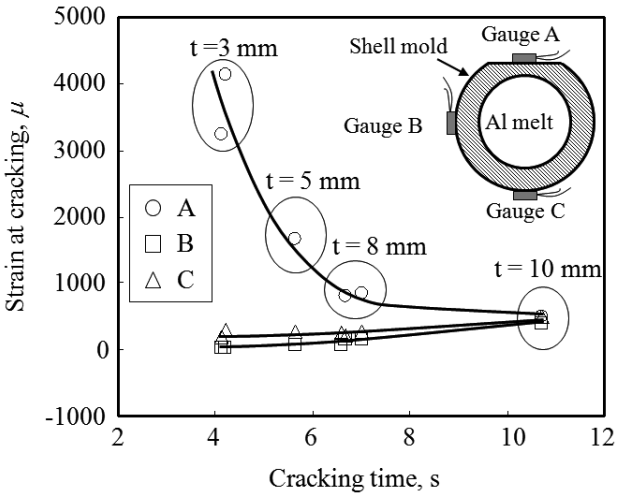

Fig. 8 Measured strains of cylindrical shell molds with thinly ground regions of different thicknesses at the time of cracking of the outer surface of the thinly ground region 60 mm above the bottom of the mold.

mold circumference. Therefore, cracks should occur if the stress corresponding to the strain in the mold exceeds the tensile strength. For the experimental mold, some irregularity in the sand filling during mold preparation is likely, and any cracking should occur at the weakest point of the mold. When a portion of the mold wall was thinly ground, a comparatively large strain was generated in the thinly ground region. This strain increased rapidly with decreasing thickness of the ground region, and led to earlier cracking during melt filling. However, the reason that the strain at cracking increased with decreasing thickness of the ground region remained unexplained.

The temperature distributions and deformation configurations of the cross sections of cup-shaped molds with and without thinly ground wall regions at cracking are illustrated in **Fig. 9**. For the unground mold (which had a uniform wall thickness of 10 mm), the cross section remained circular but was enlarged. For molds with ground regions ranging from 10 mm to 3 mm thick, the thinly ground portion deformed significantly from the initial circular shape to a shape with a larger curvature. This curvature increased with decreasing thicknesses of the thinly ground region. When the ground region was thinner than 5 mm, the increase in curvature became especially marked. Owing to the lower thickness, the thinly ground part had a bending moment that resulted in a stress gradient in the thickness direction during melt filling. This stress gradient became larger with decreasing thickness of the ground region. It is possible that it was merely this stress gradient that caused the fracture stress (strain) of the mold to be much higher than the tensile strength obtained by tensile tests. That is to say, as is generally observed for brittle materials, the bending strength is higher than the tensile strength for a given specimen size.

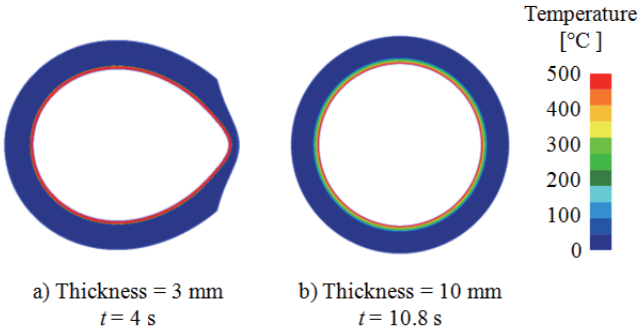

Fig. 9 Cross-sectional shapes of shell molds with thinly ground regions of different thicknesses after melt filling (100-fold amplified deformation, two-dimensional analysis).

3. 5 Criterion for Mold Cracking

For a mold that is exposed to an even distribution of tensile stress, such as in the case of the unground cup-shaped mold, the tensile strength of the mold can be considered to be the criterion for mold cracking. That is, if the tensile stress in the mold exceeds the tensile strength, then cracks will occur. However, as was observed in the above experiments, if there is a large bending moment or a severe stress gradient in a section of the mold, then the cracking stress will increase. Thus, the tensile strength obtained from a tensile test can not be used as the criterion for cracking. Therefore, the criterion for cracking under a severe stress gradient was examined using the effective volume method,[10] which is based on Weibull statistics and is used to evaluate the strength of brittle materials. The effective volume (V_E) is a parameter based on the assumption that the larger the volume under comparatively high stress in a body, the higher the probability of that volume containing relatively large defects that are capable of originating cracks. The effective volume is described by Eq. 1.

$$V_E = \int_V (\sigma/\sigma_{max})^m \, dV, \quad \cdots\cdots\cdots\cdots\cdots\cdots (1)$$

where σ is the stress in the specimen, σ_{max} is the maximum stress in the specimen, m is the Weibull parameter, and V is the total volume of the specimen.

The relationship between the mean fracture stress μ and the effective volume V_E of a brittle material can be expressed as:

$$\ln\mu = -(1/m)\ln V_E + c, \quad \cdots\cdots\cdots\cdots\cdots\cdots (2)$$

where c is a constant.

Furthermore, for a given fracture probability F, the fracture stress can be obtained from the above mean fracture stress using Eq. 3.

$$\sigma_F = \mu/S_p, \quad \cdots\cdots\cdots\cdots\cdots\cdots\cdots\cdots (3)$$

where S_p is a safety coefficient that can be calculated using Eq. 4.

$$S_p = \Gamma((m+1)/m)/(\ln(1/(1-F)))^{1/m}, \quad \cdots\cdots\cdots (4)$$

where Γ(x) is the Gamma function.

If the Weibull parameter m and the constant c are known, the relationship between the fracture stress for a given fracture probability and the effective volume can be obtained by substituting Eqs. 2 and 4 into Eq. 3. The Weibull parameter m and the constant c were calculated from the tensile test results as follows.

First, a Weilbull plot of the tensile test results was drawn as shown in **Fig. 10**. The median rank method was adopted to calculate the fracture probability, because of the small tensile test number of 10. The Weibull parameter was calculated to be 6.04 from the tangent of the Weibull plot shown in Fig. 10. This Weibull parameter is between 5 and 20,[11] which is the typical range for general ceramics, although it is at the side of a comparatively larger fluctuation.

If only the gauge length region of the tensile specimen is taken into account when calculating the effective volume of the tensile test, the effective volume simply equals the volume of the gauge length region because the stress is the same everywhere in that region, i.e., $\sigma = \sigma_{max}$ in Eq. 1. However, in the actual tensile tests, some of the specimens did not fracture in the gauge length region but in the nearby transition region. Therefore, the integration range of Eq. 1 was extended from the gauge length region to include the transition regions, and the effective volume of the tensile specimen was calculated as $V_E = 1.26 \times 10^{-5}$ m^3 (12.6 cm^3). Here, it should be noted that the cross section of the transition region was larger than that of the gauge length region, so the stress in the transition region was lower than that of the gauge length region.

By substituting $m = 6.04$, $V_E = 1.26 \times 10^{-5}$ m^3 (12.6 cm^3), and the mean tensile strength $\mu = 3.15$ MPa into Eq. 2, the constant c was obtained as c = 4.72.

The relationships between σ_F and V_E, corresponding to fracture probabilities of F = 1%, 10%, 50%, and 95% were obtained by substituting Eqs. 2 and 4 into Eq. 3. These relationships between σ_F and V_E are illustrated in **Fig. 11**, in which the fracture stress increased with decreasing effective volume. The bending strengths measured by three-point bending tests of specimens with different effective volumes are also plotted in Fig. 11 (solid circles) and showed good agreement with the fracture stresses calculated from the tensile test strengths.

The maximum principal stresses and the effective volumes at cracking were calculated for the cup-shaped molds with thinly ground regions that were used for the experiments shown in Fig. 8. The results for each mold are plotted in Fig. 11 (solid squares). The maximum principal stresses at mold cracking were located in the region of fracture probabilities of 50–95%. Therefore, the fracture stress-effective volume relationship corresponding to the fracture probability of 50% was assumed as the criterion for shell mold cracking.

3. 6 Predicting the Cracking of a Jacket Mold for Aluminum Alloy Cylinder Heads

To accurately predict the occurrence of cracks, it is first necessary to understand the detailed process by which a mold contacts the melt during casting. This was accomplished by melt filling simulation followed by the calculation of thermal stresses in the mold based on the heat transport between the mold and the melt.

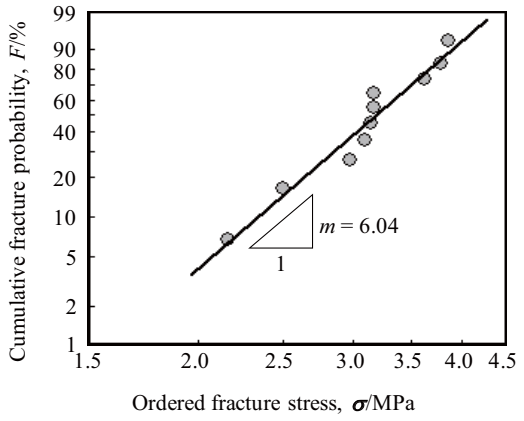

Fig. 10 Weibull plot of the fracture stresses obtained from tensile tests of the shell mold material.

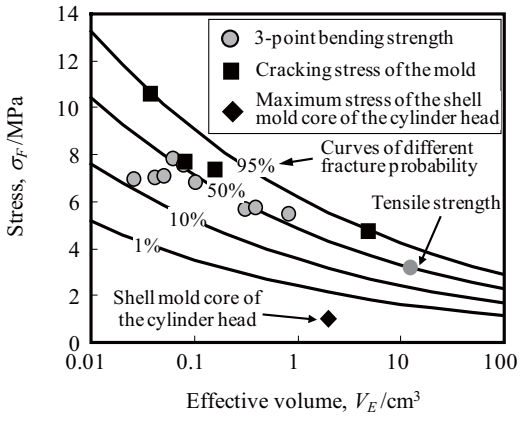

Fig. 11 Relationship between the fracture stress and the effective volume of the shell mold.

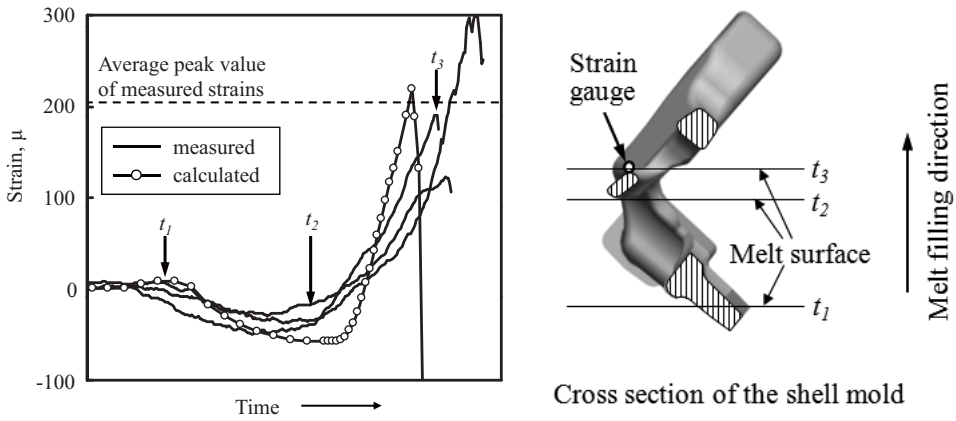

Fig. 12 Comparison of the measured and calculated strains of a jacket shell mold of a cylinder head during melt filling.

Figure 12 shows the measured strains (N = 3) in a jacket mold when it was heated by the melt as its surface rose from the lower side to the upper side of the mold vertical section. Compressive strains were measured when the surface of melt rose from t_1 to t_2. The strains began to change towards tension once the surface of the melt passed t_2, and the tensile strain continuously increased as the melt surface rose. When the melt surface arrived at the position of the installed strain gauges, the strain suddenly dropped toward the compressive side, and the strain gauges were damaged due to contact with the hot melt. The strain of the mold, calculated on the basis of a melt filling simulation using the foundry CAE software TOPCAST, is also shown in Fig. 12. The calculated strain showed a similar tendency to that of the measured strains. The distribution of the maximum principal stress in a part of the mold (the portion of one cylinder of the four cylinder head) is shown in **Fig. 13**, which shows the time at which the surface of the melt had passed t_2 and almost arrived at the position of the strain gauge shown in Fig. 12. The maximum value of the maximum principal stress was approximately 1 MPa, which was much lower than the tensile strength of the mold, and was located at a position with a fracture probability lower than 0.01%, according to Fig. 11. Therefore, the risk of cracking is extremely low under the present casting conditions.

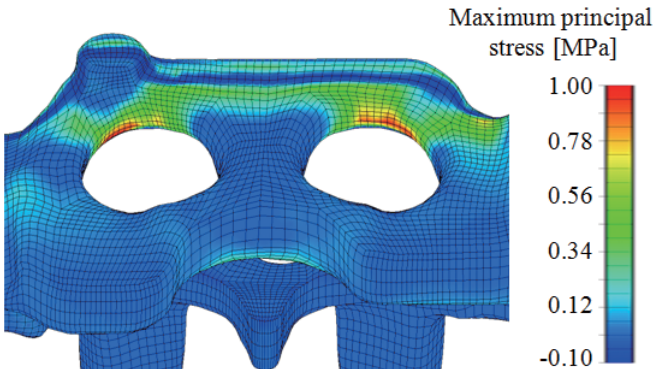

Fig. 13 Stress distribution in a jacket shell mold of a cylinder head during melt filling at t_3 in Fig. 12.

4. Conclusions

The cracking of shell molds during the casting of JIS-AC4C aluminum alloy was investigated, with a focus on the thermal stress in the mold arising from melt heating. The following conclusions were obtained.

1. The temperature of the inner side of the cup-shaped mold increased due to heating by the aluminum melt. The thermal expansion of the inner side corresponding to this temperature increase was restrained by the outer side of the mold that remained at a lower temperature, resulting in compressive and tensile stresses in the inner and outer sides of the mold, respectively. The tensile stress in the outer side of the mold can rise to a high level in a short time. If this tensile stress exceeds the tensile strength of the mold, cracking will occur.
2. Even if tensile stress occurs in the outer side of a mold, if that side is heated by the melt before the stress exceeds the tensile strength, the tensile stress will decrease rapidly, and no cracking will occur.
3. For a cup-shaped mold with a thinly ground region, cracks occurred in the thinly ground part, and the cracking time decreased with decreasing thickness of the thinly ground part.

4. In a mold with a thinly ground part, the maximum tensile stress occurred in the thin region, and cracks occurred in this region. The cracking stress (strain) increased with decreasing thickness of the thinly ground part.
5. The cracking criterion for shell molds can be described by the effective volume method, which is used to assess the strength of brittle materials and is based on Weibull statistics. Whether cracks will occur can be predicted by comparing the tensile stresses in the surfaces of molds with the fracture stress (strength) of the same effective volume, which can be obtained from a graph of the fracture stress-effective volume relationship based on tensile or bending tests.
6. The proposed cracking criterion in the present research was successfully applied to predict the cracking of water jacket molds in the casting of automotive cylinder heads.

Acknowledgements

The authors are grateful to the people of SANEI SILICA Ltd., Japan for their help in the measurement of shell mold properties.

References

(1) Campbell, J., *CASTINGS* (1991), 98, Butterworth-Heinemann Ltd.
(2) Makiguchi, T., *IMONO* (in Japanese), Vol.62 (1990), p.566.
(3) Oota, H., Sakaguchi, Y., Kuniyoshi, K. and Murata, H., *Report of JFS Meeting* (in Japanese), Vol.152 (1979), p.48.
(4) Morey, R. E., *Trans. AFS*, Vol.54 (1949), p.129.
(5) Katashima, S., Tashima, S. and Mikawa,Y., *Report of AFS Meeting*, Vol.113 (1988), p.91.
(6) Nakano, T., Muto, K. and Tanabe, H., *IMONO* (in Japanese), Vol.50 (1978), p.36.
(7) Yajima, M. and Hase, H., *IMONO* (in Japanese), Vol.55 (1983), p.765.
(8) Onaka, I., *Journal of Japan Foundry Engineering Society* (in Japanese), Vol.78 (2006), p.602.
(9) Otsuka, Y., *Journal of Japan Foundry Engineering Society* (in Japanese), Vol.78 (2006), p.609.
(10) The Ceramic Society of Japan, *The Mechanical Properties of Ceramics* (in Japanese), (1979), p.22.
(11) Davidge, R. W., (Translated by Suzuki, H. and Iseki, T.), *The Strength and Fracture of Ceramics* (in Japanese), (1982), p.147, Kyoritsu Shuppann.

Figs. 1-13 and Table 1
Reprinted from Materials Transactions, Vol.51, No.8 (2010), pp.1420-1427, Dong, S., Iwata, Y., Hohjo, H., Iwahori, H., Yamashita, T. and Hirano, H., Shell Mold Cracking and Its Prediction during Casting of AC4C Aluminum Alloy, © 2010 JFES, with permission from Japan Foundary Engineering Society.

Shuxin Dong
Research Fields:
- Metallic Materials
- Modeling of Casting and Solidification Processes

Academic Degree: Dr. Eng.
Academic Societies:
- The Japan Institute of Metals
- Japan Foundry Engineering Society
- The Surface Finishing Society of Japan

Awards:
- The Tsutsumi Award of Japan Foundry Engineering Society, Tokai, 2005
- The Best Paper Award of Japan Foundry Engineering Society, 2010

Yasushi Iwata
Research Field:
- Modeling of Casting and Solidification Processes

Academic Degree: Dr. Eng.
Academic Society:
- Japan Foundry Engineering Society

Awards:
- The Onoda Award of Japan Die Casting Association, 1989
- The Kobayashi Award of Japan Foundry Engineering Society, 1989
- The Tsutsumi Award of Japan Foundry Engineering Society, Tokai, 1999
- The Best Paper Award of Japan Foundry Engineering Society, 2001 and 2010

Hiroshi Hohjo
Research Fields:
- Material Strength
- Fracture Mechanics

Academic Degree: Dr. Eng.
Academic Societies:
- The Society of Materials Science, Japan
- The Japan Society of Mechanical Engineers

Award:
- JSMS Award for Technical Developments, 2007

Hiroaki Iwahori

Research Field:
- Casting Technology and Materials

Academic Degree: Dr. Eng.

Academic Societies:
- Japan Foundry Engineering Society
- The Japan Institute of Light Metals
- The Japan Institute of Metals

Awards:
- The Sokeizai Industrial Technology Award, 1991
- The Best Technical Paper Award of the 62th World Foundry Congress, 1996
- The Iidaka Award of Japan Foundry Engineering Society, 2009
- The Technological Development Award of Japan Foundry Engineering Society, 2010
- The Best Paper Award of Japan Foundry Engineering Society, 2001 and 2010

Takashi Yamashita*

Research Field:
- CAE of Casting Processes

Academic Society:
- Japan Foundry Engineering Society

Awards:
- The Technological Development Award of Japan Foundry Engineering Society, 2009
- The Encouragement Award of Japan Foundry Engineering Society, Tokai, 2011

Haruyoshi Hirano*

Research Fields:
- Foundry Engineering
- Quality Engineering
- Production Management

Academic Societies:
- Japan Foundry Engineering Society
- The Japan Society for Quality Control

Awards:
- The Toyota Award of Japan Foundry Engineering Society, 1998
- The Technological Development Award of Japan Foundry Society, Inc., 1999
- The Nagai Technological Development Award of the Nagai Foundation for Science and Technology, 2004
- The Technological Development Award of Japan Foundry Engineering Society, 2010
- The Distinguished Contribution Award of Japan Foundry Engineering Society, 2011

*Toyota Industries Corporation

